Computational Angle of Arrival Detection Using Dynamic Metasurfaces

(Invited Paper)

Idban Alamzadeh, Travis Williams, and Mohammadreza F. Imani School of Electrical, Computer, and Energy Engineering Arizona State University, Tempe, AZ 85287, USA, Email: Idban.Alamzadeh@asu.edu and Mohammadreza.imani@asu.edu

Abstract—Detecting the direction of wireless signals across the entire horizon can greatly benefit various wireless communication and sensing systems. While traditional phased antenna arrays and mechanically rotating sensors can achieve the desired performance, they often come with drawbacks such as high cost, bulkiness, excessive weight, or high power consumption. Additionally, mechanical and stealth requirements necessitate that antenna hardware be embedded within shapes that conform to the surfaces of objects. To address these issues, we propose and numerically demonstrate conformal dynamic metasurface antennas that can wrap around arbitrary objects. These antennas can generate diverse patterns that interrogate the entire field of view, allowing for multiplexing relevant information into a few measurements at a single receiving unit. We will detail its design considerations and outline methods for computationally processing signals collected by this device to extract the angles of arrival of one or multiple signals. The proposed structure represents a new approach to designing microwave sensors for acquiring situational awareness.

I. INTRODUCTION

Microwave sensing systems map the surrounding environment, find obstacles, detect threats, identify RF sources, and provide the required situational awareness [1]–[15]. They usually need to be mounted on structures such as vehicles, missiles, drones, helmets. etc., where mechanical and stealth restrictions require them to be embedded into arbitrarily shaped surfaces. Another requirement is to gather real-time information across the entire field of view (e.g., in the azimuth plane) while using as few transceivers as possible. Traditionally, this has involved either mechanically rotating antennas or employing conformal antenna arrays. While these methods can deliver excellent performance, they may also lead to concerns such as bulkiness, high costs, excessive power consumption, increased weight, or slower operation, which can limit their widespread applications.

Microwave sensors that use rotating radars provide a one-to-one relationship between each measurement and the interrogated angle/pixel [1], [2], [15]. As a result, they provide perfect performance but at the cost of a bulky, and heavy instrument. Rotating antenna systems are also challenging in conforming to arbitrary shapes. Alternatively, one can use antenna arrays that are electronically switched on and off or fed via a specialized feed [7], [16], [17]. Conformal antenna arrays can interrogate a large field of view and are easier to integrate

into arbitrarily shaped objects. However, their performance requires satisfying important element gain and array spacing tradeoffs [18], [19]. Furthermore, almost all previous methods require using a transmitting/receiving unit connected to one of the antennas (or a switch array), increasing the overall cost and complexity. To overcome that issue, compressive sensing algorithms or machine learning techniques have been proposed to reduce the number of measurements, especially with pattern reconfigurable antennas, but they still require conventional antenna arrays with their C-SWaP issues [20]–[23].

To address these shortcomings, a conformal frequencydiverse metasurface antenna has been recently pursued [24]. The underlying idea behind this device is to generate angularly diverse radiation patterns that can multiplex information about the incident angle of arrival (AoA) [24] into fast frequency sweeps. In this case, there is no one-to-one relationship between measurements at the receiving ports and the incoming signal's AoA. Instead, the AoA is determined using computational techniques. Using full-wave simulations, [24] demonstrated the capability of a frequency-diverse conformal antenna in detecting any incoming signal's AoA on the azimuth plane. Nevertheless, the frequency-diverse metasurface relies on a large bandwidth, which limits its application. To overcome this limitation, recent work also examined a dynamic conformal metasurface by adding a reconfigurable component into each element of the conformal frequency diverse metamaterial antenna [25]. This work presented the possibility to detect AoA even using a single frequency. However, the proposed geometry was not physically realizable (it required large capacitors of a few Farad to realize the reconfigurable element).

Building upon the work in [25], we present a conformal dynamic metasurface antenna (DMA) optimized for generating diverse patterns and detecting many AoAs. We will start by outlining the design considerations for the constitutive elements of the proposed DMA. Next, we will analyze the overall electromagnetic response of the conformal DMA. We will also describe the processing technique for determining the AoA using measurements made by this device. Using electromagnetic full-wave simulations in Ansys HFSS, we demonstrate the ability to detect single and multiple AoAs. Additionally, we show that it is possible to use intensity-only

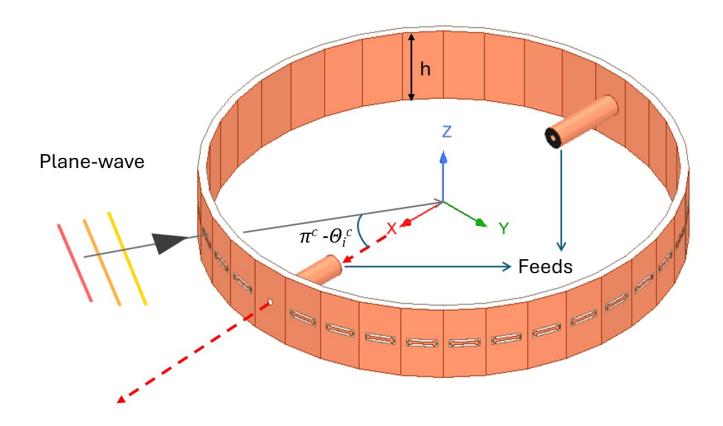


Fig. 1. The conformal DMA.

measurements (i.e., received signal strength) to detect AoA across the entire horizon.

II. PROPOSED METHOD

The general configuration of the proposed conformal DMA is shown in Fig. 1. It consists of a conformal substrateintegrated waveguide (SIW) with one wall fashioned with reconfigurable metamaterial radiators whose response can be tuned individually [26]. This SIW is connected to two coaxial connectors on opposite sides. An electromagnetic wave incident on this structure couples to the metamaterial radiators (depending on their switchable component state) and travels along the SIW to be collected by the coaxial connectors. The received signal is thus a linear weighted combination of the wave incident on all metamaterial elements. The random weights depend on the state of the material elements and their distance from the coaxial connector [27]. We can obtain a new multiplexed version of the incident signal by changing the metamaterial radiators' states. By computationally analyzing the signal measured in this manner, we can obtain the AoA of the incident signal. In the following, we first detail the design considerations for the dynamic elements used as the building block of this antenna. We then analyze the electromagnetic response of the conformal DMA composed of the designed dynamic elements. Lastly, we outline the signal processing technique to obtain AoAs and verify it using full-wave simulation.

A. Element design

The constituting element of the conformal DMA is shown in Fig. 2. It is excited by a SIW implemented using a 62 mil thick Rogers Duroid 5880 substrate. A portion of the guided mode traveling within the SIW couples to the element and radiates into free space. This element is loaded with two varactor diodes, which can be addressed individually. Thus, the resonance behavior of the element can be tuned according to the state of these two diodes. In this paper, we design the element to be resonant in the X band. It is worth noting that the proposed design and operation can be easily extended to other frequencies by altering the element's geometry. To simplify

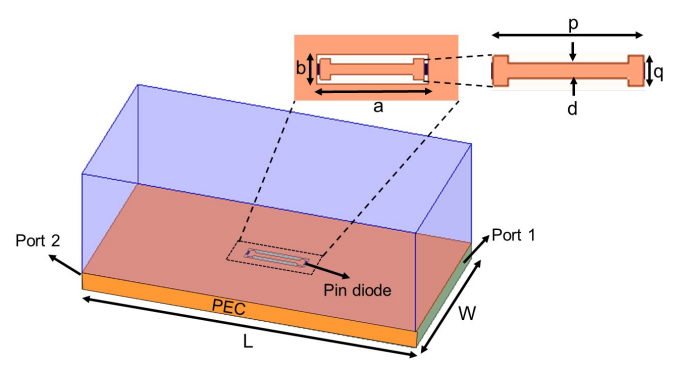


Fig. 2. The simulation setup of a DMA element with dimensional details.

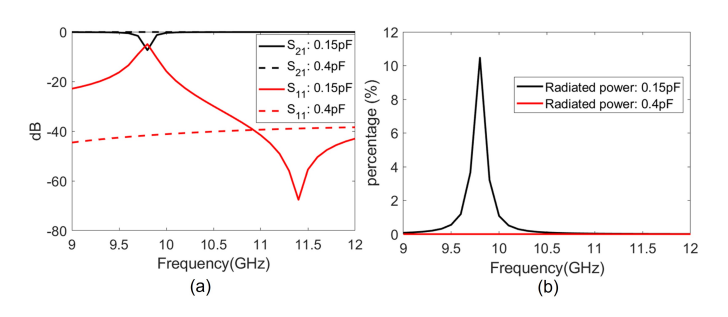


Fig. 3. The a) S-parameters and b) radiated power of a single meta-atom.

simulation studies, the walls of the SIW are modeled as perfect electric conductor boundary conditions. The SIW's width is W = h = 15 mm, corresponding to a cutoff frequency of 6.74 GHz. For the design analysis of the element, we excite it with a rectangular waveguide port. The corresponding scattering parameters thus provide us with metrics to optimize the design. Specifically, we want to satisfy two conditions: 1) low reflection, measured by S_{11} , and 2) low coupling, measured by S_{21} . These two conditions ensure sufficient power reaches subsequent elements along the DMA, allowing us to use the DMA aperture effectively [28]. To meet these criteria, we used elements with narrow widths, which reduces the perturbation of the guided mode by the element and lowers reflection. This also reduces the coupling, allowing sufficient power to pass through the element to excite subsequent elements. Using a parametric study in Ansys HFSS, we arrived at the following geometrical parameters: a = 5.4 mm, b = 1.4 mm, p = 5 mm, q = 1 mm, and d = 0.5 mm.

Fig. 3a depicts the S-parameter for the optimized element for two capacitance values of the varactor diodes. The first state, $C=0.15 \mathrm{pF}$, is chosen such that the element resonates at 9.8GHz. In contrast, for the second state, $C=0.4 \mathrm{pF}$, the resonance frequency is effectively shifted out of the band of operation. This selection thus allows for a binary coding of the conformal DMA. This response is also apparent from the radiated power depicted in Fig. 3b.

B. Conformal DMA

The conformal DMA is formed by placing the elements designed in the previous subsection around a cylindrical struc-

ture so that the elements radiate radially outward. The outer radius of the cylindrical structure is 45 mm. This structure, depicted in Fig 1, is excited by two coaxial ports placed on opposite sides. The center conducting cores of the connectors extend through the substrate. The conformal DMA is tasked with capturing signals from the whole 360° angular range on the horizontal plane (XY plane in Fig 1). In this configuration, the angular range on the azimuth plan is $[-180^{\circ}, 180^{\circ}]$, with the X-axis at -180° . Given the metamaterial elements' orientation, we assume the incident waves have an electric field in the horizontal plane.

Placing the metamaterial elements on a conformal configuration in series with each other can slightly change their response. To analyze that, we examined the S parameters of this structure. The design criteria in these studies are as follows: 1) The reflection coefficient should be low to ensure sufficient signals are received from the elements. 2) The transmission from one port to the other should be low so that the signal is depleted before reaching the second port (all of it is radiated). 3) The overall radiation patterns of the antenna cover the whole horizon and do not exhibit significant nulls. The critical challenge here is that all these conditions must be satisfied for all different states of the varactor diodes along the conformal DMA.

For simplicity, we only used two states for each diode: their effective capacitance is either 0.15 pF or 0.4 pF based on the studies presented above. Even in this case, we still have 2^{34} possible distribution of effective element states (referred to as *masks* for brevity), which cannot be examined in simulation (or experiment). It is worth noting that this large number of possible states shows the dexterity of the designed DMA. To overcome this challenge, we grouped the metamaterial elements into 5 groups. The elements of each group will have the same capacitance (or, equivalently, will have the same voltage exciting them). These elements are randomly distributed over the whole DMA. Using these groups, the total number of masks to simulate will be 31—we disregard the case where all elements are loaded with 0.4 pF since it corresponds to the case that they are effectively off.

In Figs 4a, c, and e, the reflection and transmission coefficients as a function of masks at different frequency points are plotted. As expected, we see that both reflection and transmission are heavily dependent on the mask. We can also observe that they change as a function of frequency. Figs 4b, d, and f depict the radiated power for the same set of masks and frequency points. Similar to the S-parameters, we can notice the fluctuation of the radiated power across the masks. Near the expected resonance frequency, i.e. 9.8 GHz, we observe high transmission from one port to another port, while radiated power is low. We thus can conclude that the resonance frequency of the elements has slightly shifted. By observing the S parameters and radiated power at 9.65 and 9.5 GHz, we can conclude the resonance frequency is lower than 9.8 GHz. It is worth emphasizing that the exact resonance frequency is not an important factor in determining the frequency of operation. In fact, we expect the device to

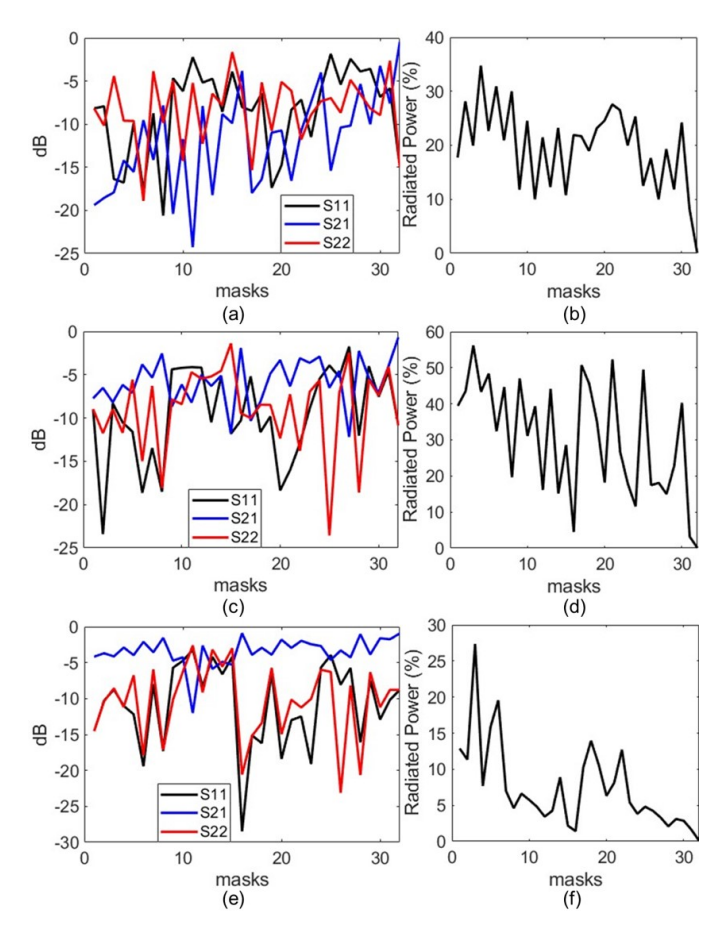


Fig. 4. The S-parameters (left) and the percentage of the radiated power (right) of the conformal DMA when both ports are excited simultaneously at a)-b) 9.5 GHz, c)-d) 9.65 GHz, and e)-f) 9.8 GHz.

outperform slightly off the resonance frequency where losses are lower, and the perturbation of the guided wave is less. As a result, each element would exhibit lower reflection and allow for ample signal to transfer to the subsequent elements. Our main factor in determining the frequency of operation is the amount of radiated power, which is higher (on average) for 9.65 GHz.

We have plotted the radiation patterns of the DMA across all the masks for the same frequency points in Fig 5. These radiation patterns are also accompanied by their envelopes in Fig 5 (denoted by the thick black line). Changing masks results in angularly diverse radiation patterns, while the combination of the masks shows the ability to receive signals from all angles. It is worth noting that the envelop pattern exhibits deeper minimums at 9.8 GHz. In other words, it does not receive signals from certain angles with the desired power. Combining the results of Fig 5 and Fig 6, we concluded that operating at 9.65 GHz can provide the desired performance, which will be used for the rest of this paper. It is worth emphasizing that this is a qualitative argument. One may find slightly better performance at other frequencies (e.g., 9.7 GHz or 9.6 GHz). Finding the optimum frequency is left for future work. We focus here on showcasing the capabilities of a

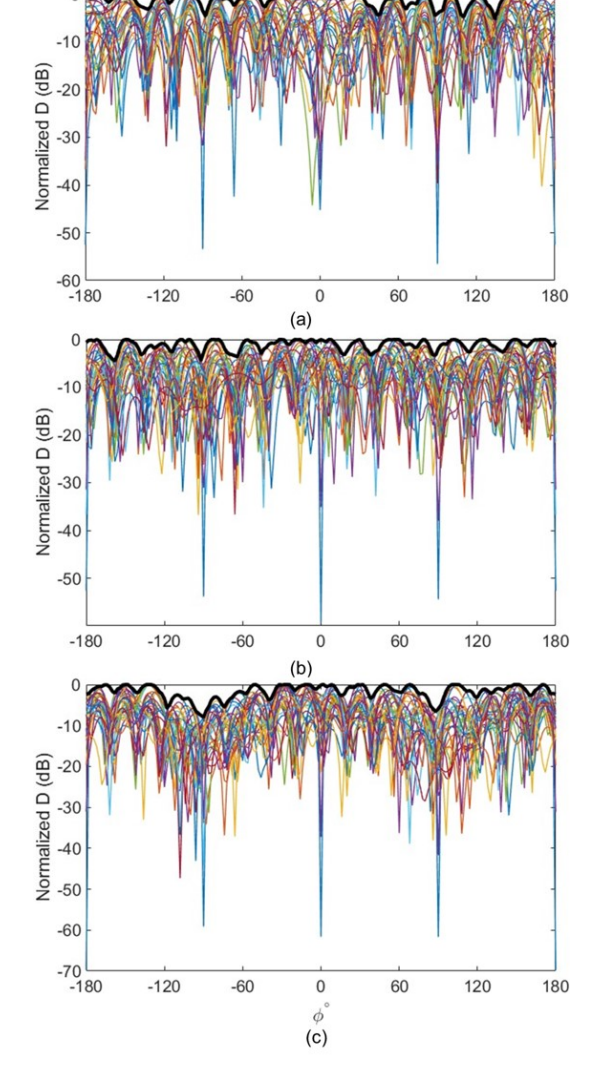


Fig. 5. Normalized radiation patterns for the Conformal DMA at a) 9.5 GHz, b) 9.65 GHz and c) 9.8 GHz with 31 masks. The envelopes of the patterns are denoted with a thicker black line.

conformal DMA in detecting AoAs. It is also worth noting that this selection was based on the particular set of masks consisting of 0.15 pF and 0.4 pF. The optimum frequency can be changed to other values using masks with different sets of capacitors. Alternatively, if we used a more continuous range of capacitors, we could obtain the desired performance for a wide band of operation. This will be especially useful if we also want to locate the source in the range. These efforts are left for future work.

III. COMPUTATIONAL AOA DETECTION

A. Detection using complex data

To detect AoA using the diverse reception patterns generated by the conformal DMA, we adopt a procesure similar to the one used in [24], [29], [30]. The initial step is to discretize the whole azimuth range, -180° to 180° into discrete bins. The number of bins N may be selected such that the angular

difference between the center of adjacent bins is not larger than the half-power-beamwidth (HPBW) of the antenna. The beamwidth of this conformal antenna is estimated to be 13.5° based on the numerical calculation for a circular array. However, we can detect the AoA with better resolution since we assume that the number of predominant signal incidents on the device is known (as a priori knowledge). As a result, we divided the whole azimuth range into N=60 bins, resulting in a dense discretization (bin size of 6° instead of 13.5°).

We characterize the conformal DMA by illuminating it with plane wave incident from the directions at the center of the N bins. The signal incident from each reference angle is sampled separately from the two ports for 31 masks described earlier. Then, we take the difference between the sensed data to populate a reference matrix \mathbf{H} . In practice, this difference calculation process can be accomplished by numerically performing the subtraction in the post-measurement step using a simple microprocessor. Alternatively, one can include an RF component, such as a 180 degree hybrid coupler, to take the difference between the collected signals. In our simulation, we mimicked the former way for AoA estimation:

$$\mathbf{y}_{test} = \mathbf{y}_{port1} - \mathbf{y}_{port2}.\tag{1}$$

It should be noted that the subtracted value is a complex number. We repeated this process for the 31 masks and N=60 AoAs to populate a reference matrix $\mathbf{H}_{M\times N}$ where M=31

To ensure the formulation of a robust and useful estimation algorithm, the columns of **H** must be sufficiently distinct such that we can detect the unknown incident signal's AoA by correlating the columns of **H** with the measured signal. This is critical because the received data from the whole conformal DMA is captured only using two ports. This may result in insufficient information for accurate AoA estimation. As a result, the estimation process relies highly on the diversity of the received information from different masks. Therefore, we first verified that each mask contributes relatively new information by computing the singular value decomposition (SVD) of **H**. We then plotted SVDs for increasing rows of **H** and observed a decreasing trend in the slopes of the SVD, indicating newer information is being added with new masks. A few examples of this study are shown in Fig 6a.

To verify the AoA detection, we used the reference AoA set as well as an arbitrary set of AoAs that are not within the reference AoAs. In addition, it is crucial to assess the AoA detection capability at different radial distances. We emulated that by multiplying each test data \mathbf{y}_{test} with random magnitude and phase variations:

$$\mathbf{y} = A_{rand} \mathbf{y}_{test} e^{j\phi_{rand}} \tag{2}$$

Where $A_{rand} \in [0.5, 0.98]$ and $\phi_{rand} \in [0^{\circ}, 360^{\circ}]$ are the imposed amplitude and phase values respectively. The resulting dataset \mathbf{y} has the same size as \mathbf{y}_{test} which is a complex-valued vector of length $M \times 1$. The random phase and amplitude emulate signals originating from a random radial

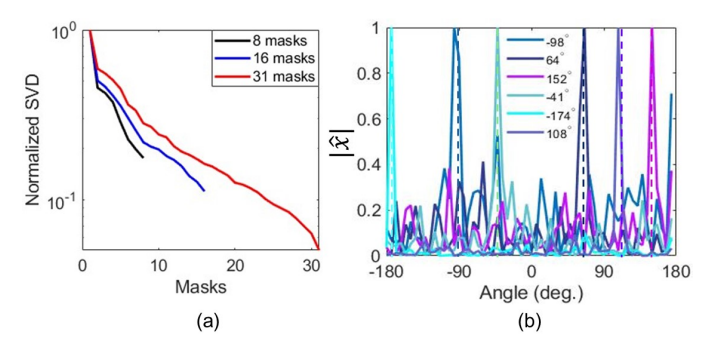


Fig. 6. a) Normalized singu; ar values for increasing number of masks. b) Normalized $|\hat{\mathbf{x}}|$ for different test angles. The actual AoAs are noted with dashed lines.

distance. The perturbed sensed data is then related to the incident signal using the following estimation problem:

$$y = Hx (3)$$

Where x is the parameter to be estimated and has values of 1 only at the indices corresponding to the actual AoAs and zeros otherwise. Since the reference matrix is not square, we need to solve equation (3) computationally. In this paper, we use MATLAB built-in least square solver, CGS, to obtain an estimate of x, which we will denote as \hat{x} . Ideally, \hat{x} should perfectly mirror x. In reality, however, the test data is disrupted by noise. This disruption is manifested in the magnitude and phase variation in the sensed complex data. As such, the estimated $\hat{\mathbf{x}}$ is not comprised of only 0s and 1s. In fact, there is a possibility of redundant peaks in $\hat{\mathbf{x}}$. However, in most working conditions, the peaks corresponding to incident AoAs should be easily distinguishable, as shown in Fig 6b. Here, $|\hat{\mathbf{x}}|$ for a set of AoAs are presented in one figure. Clearly, peaks at the corresponding angles are significantly higher than the redundant ones, proving the detectability of AoA.

It is worth mentioning that the test AoAs in Fig 6b is not from the reference AoA set. Therefore, one may notice a slight deviation of the estimated AoA from the actual AoAs. However, this deviation is acceptable as long as it is less than the HPBW of the antenna. Therefore, an estimated AoA is considered accurate if it is within the \pm HPBW of the actual AoA, which is around 6.7° according to an earlier discussion.

In Fig 7, we plotted estimated AoAs vs. actual incident AOAs for a dense set of AOA in $[-180^{\circ}, 180^{\circ}]$. In Fig 7a, we analyzed the estimation performance at 15 dB SNR. Evidently, all the AoAs are detected perfectly and the differences between the estimated and corresponding test AoAs are much less than the HPBW. It is crucial to remember that each sensed test data is already perturbed with random magnitude and phase (see equation (2)). In all the studies of noise levels in this paper, the SNR values are applied to this perturbed data:

$$\mathbf{y}_{noisy} = \mathbf{y} + \tilde{w} \tag{4}$$

Where \tilde{w} is white Gaussian noise of a certain SNR level. As the SNR decreases, the difference between the redundant

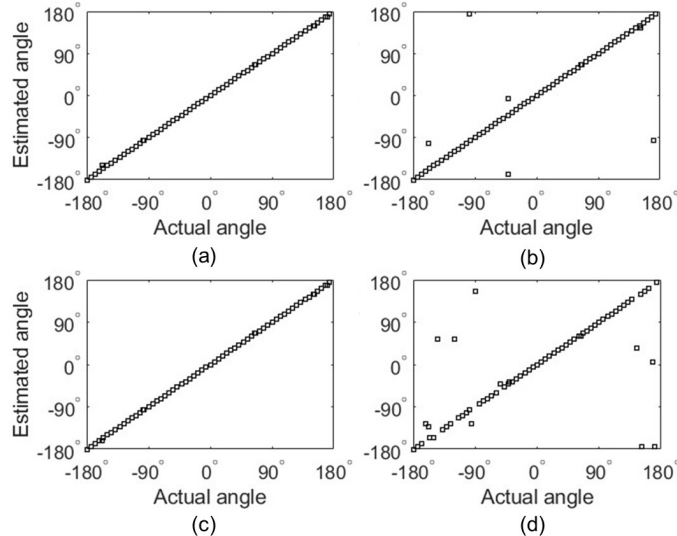


Fig. 7. Estimated AoA vs. actual AoA under different scenarios with a) 31 masks at 15 dB SNR, b) 31 masks at -10 dB SNR, d) 16 masks, and e) 8 masks, both at 15 dB SNR.

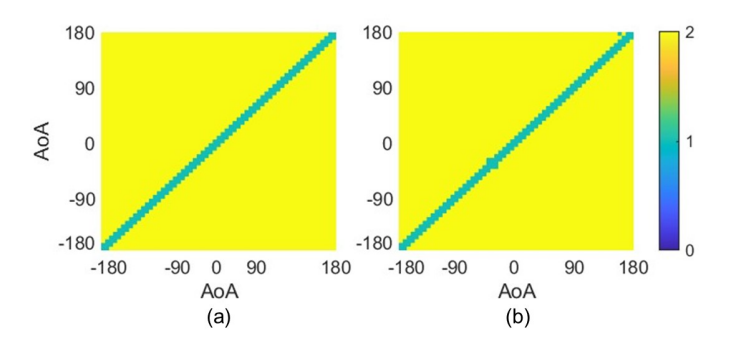


Fig. 8. Accuracy of estimation of two AoAs in a) a noiseless setting, and b) in a noisy setting with 15 dB SNR. The color bar reflects the number of accurately estimated AoA(s).

and main peaks decreases. At low SNR values, around -10 dB or lower, we notice unreliable detection for several AoAs, as shown in Fig 7b.

Another important factor in the estimation performance is the number of masks, M. We have examined the estimation accuracy while decreasing the number of masks in Fig 7 (c) and (d). In both of these figures, the SNR level is kept the same at 15 dB. We can see that there is no noteworthy deviation in AoA detection capability when the number of masks is reduced to 16. The estimation performance degrades substantially when the number of masks is reduced to 8.

Next, we examine the conformal DMA's capability of detecting multiple AoAs. To emulate multiple incident signals, we invoke the principle of superposition, where the sensed data from I incoming signals can be described as:

$$\mathbf{y} = \sum_{i=1}^{I} A_{i,rand} \mathbf{y}_{i,test} e^{j\phi_{i,rand}}$$
 (5)

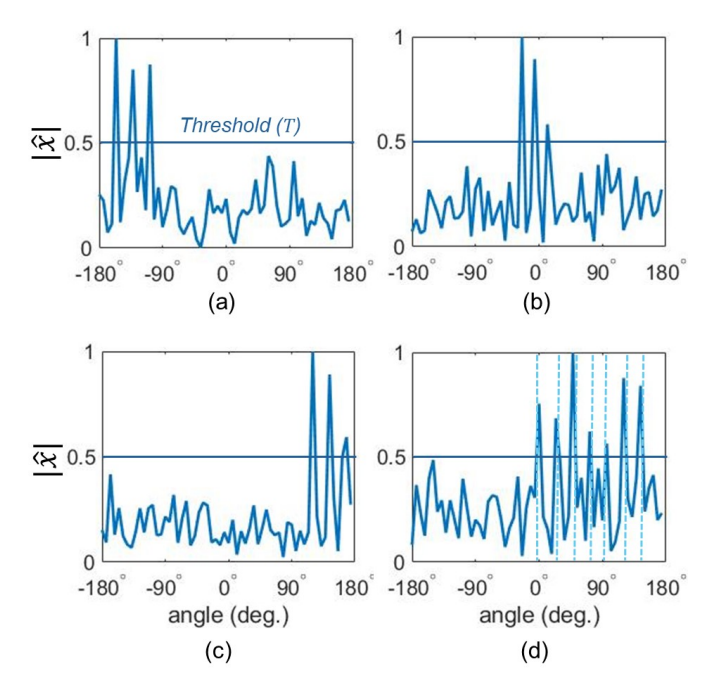


Fig. 9. Normalized $|\hat{\mathbf{x}}|$ for incident signals at a) -156° , -132° and -108° , b) -24° , -6° and 12° , and c) 120° , 144° and 168° . d) Normalized $|\hat{\mathbf{x}}|$ for a dense set of incident signals. All the plots were derived at 15 dB SNR.

Each incoming signal may be perturbed by a different magnitude and phase. For simplicity, we assume all incoming signals are multiplied by the same random magnitude and phase. The sensed data computed using equation (5) is then used in equation (3) which is solved to find the estimated, $\hat{\mathbf{x}}$. We have plotted the estimation accuracy for two incoming signals (i.e. I=2) in Fig 8. In this figure, 0, 1, and 2 represent no detection, single AoA detection, and two AoA detections, respectively. We have conducted this test for every possible combination of reference angles. Fig 8a depicts the estimation performance assuming no noise while the performance in the presence of 15 dB SNR is shown in Fig 8b. Almost every combination of two AoAs can be successfully estimated using the conformal DMA, except for the ones that are too close to each other.

As the number of possible AoA increases, the problem of associating a peak with a possible AoA becomes more complicated. This is because the height of redundant peaks starts to become comparable to the peaks corresponding to the actual AoA. We thus need a protocol to distinguish them. For that purpose, we used a threshold to set the lower bound of detection. We empirically found that setting the threshold at the 50% of the maximum of $|\hat{\mathbf{x}}|$ can serve the purpose of AoA detection. We illustrated detections of several sets of three AoAs in Fig 9. Evidently, the peaks corresponding to the actual AoAs are distinctively above the threshold. We also observe the possibility of detecting 7 AoAs. However, as the number of AoAs increases, the inverse problem at the heart of AoA estimation becomes more complicated. As a result, more erroneous detection appears. The maximum number of AoAs

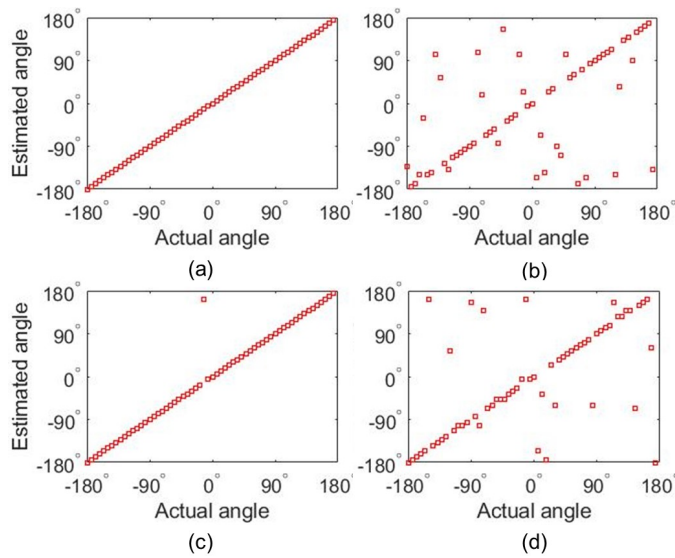


Fig. 10. Intensity-only estimated AoA vs. actual AoA with a) 31 masks at $15~\rm dB~SNR,~b)$ 31 masks at $-10~\rm dB~SNR,~d)$ 16 masks, and e) 8 masks, both at $15~\rm dB~SNR.$

this device can detect will depend on the number of masks, the noise level, and the reconstruction technique. Investigating this limit will be an interesting topic of research in the future.

B. Phaseless AoA detection

As emphasized in [30], [31], the capability to detect AoAs using intensity-only measurements (or received signal strength) eliminates the necessity of phase detection, significantly simplifying the receiving circuitry. To test this possibility, we emulated the detection of intensity data by taking the magnitude of the complex sensed data in (2). Thus, we recast each sensed data and the reference matrix $\mathbf{H}_{intensity}$, which are now comprised of real-valued entries. The inverse estimation problem then becomes:

$$\mathbf{y}_{intensity} = \mathbf{H}_{intensity} \mathbf{x},$$
 (6)

where x is similar as before. We solved the estimation problem using CGS. In these studies, the SNR is defined by adding white Gaussian noise to the complex data before computing the magnitude. We have plotted the outcomes of the intensity-only AoA estimation in Fig 10. As shown in Fig 10a, we can obtain perfect estimation performance at 15 dB SNR with 31 masks. In Fig 10b, the impact of noise is visible as with the same number of masks, the estimation performance is degraded significantly at -10 dB SNR. Next, we analyzed the impact of number masks. The estimation performance did not change as the number of masks was reduced to 16, as shown in Fig 10c. However, when the number of masks is reduced to 8, the estimation is severely degraded, as shown in Fig 10d.

IV. CONCLUSION

We presented a novel conformal DMA that can be used for AoA detection over the whole horizon using only a single receiving unit without requiring a mechanical or electronic beam steering mechanism. We outlined and verified the algorithm for using this device to detect single or multiple AoAs. The results and the analyses provided here also lead to several open research questions. One area to explore is the limit of detectable AoAs for a given diameter of the DMA. Another question is whether we can use more than a single frequency to increase sensing fidelity or obtain range information. Moreover, an open question is whether this device can be used for imaging purposes [32], i.e., to obtain reflectivity maps in the range and angular directions. The proposed conformal DMA can find applications in radar and surveillance systems, wireless communication networks, or for obtaining situational awareness.

ACKNOWLEDGMENT

This material is based upon work supported by the National Science Foundation under Grant No. ECCS-2333023.

REFERENCES

- H. Klausing, "Feasibility of a synthetic aperture radar with rotating antennas (rosar)," in 1989 19th European Microwave Conference. IEEE, 1989.
- [2] D. Vivet, P. Checchin, and R. Chapuis, "Localization and mapping using only a rotating fmcw radar sensor," *Sensors*, vol. 13, no. 4, pp. 4527– 4552, 2013.
- [3] F. Ali, G. Bauer, and M. Vossiek, "A rotating synthetic aperture radar imaging concept for robot navigation," *IEEE transactions on microwave* theory and techniques, vol. 62, no. 7, pp. 1545–1553, 2014.
- [4] Y. Wang, Q. Song, J. Wang, and H. Yu, "Airport runway foreign object debris detection system based on arc-scanning sar technology," *IEEE Transactions on Geoscience and Remote Sensing*, vol. 60, pp. 1–16, 2022.
- [5] M. Adams and M. D. Adams, Robotic navigation and mapping with radar. Artech House, 2012.
- [6] S. Lee, S.-Y. Kwon, B.-J. Kim, H.-S. Lim, and J.-E. Lee, "Dual-mode radar sensor for indoor environment mapping," *Sensors*, vol. 21, no. 7, p. 2469, 2021.
- [7] M. Angelilli, L. Infante, and P. Pacifici, "A family of secondary surveillance radars based on conformal antenna array geometries," in 2017 IEEE Radar Conference (RadarConf). IEEE, 2017, pp. 1681– 1694
- [8] P. D. Peshwe, A. G. Kothari, I. S. Darwhekar, and A. M. Chauhan, "Threat detection with millimeter wave conformal antenna array using beamforming and direction of arrival estimation," *International Journal* of RF and Microwave Computer-Aided Engineering, vol. 32, no. 3, p. e23030, 2022.
- [9] M. Meyer and G. Kuschk, "Automotive radar dataset for deep learning based 3d object detection," in 2019 16th european radar conference (EuRAD). IEEE, 2019, pp. 129–132.
- [10] M. Moallem and K. Sarabandi, "Polarimetric study of mmw imaging radars for indoor navigation and mapping," *IEEE transactions on antennas and propagation*, vol. 62, no. 1, pp. 500–504, 2013.
- [11] A. Venon, Y. Dupuis, P. Vasseur, and P. Merriaux, "Millimeter wave fmcw radars for perception, recognition and localization in automotive applications: A survey," *IEEE Transactions on Intelligent Vehicles*, vol. 7, no. 3, pp. 533–555, 2022.
- [12] T. Grebner, P. Schoeder, V. Janoudi, and C. Waldschmidt, "Radar-based mapping of the environment: Occupancy grid-map versus sar," *IEEE Microwave and Wireless Components Letters*, vol. 32, no. 3, pp. 253–256, 2022.
- [13] R. Rouveure, P. Faure, and M.-O. Monod, "Description and experimental results of a panoramic k-band radar dedicated to perception in mobile robotics applications," *Journal of Field Robotics*, vol. 35, no. 5, pp. 678–704, 2018.
- [14] Y. Nan, X. Huang, and Y. J. Guo, "A panoramic synthetic aperture radar," *IEEE Transactions on Geoscience and Remote Sensing*, vol. 60, pp. 1–13, 2022.

- [15] P. Stockel, P. Wallrath, N. Pohl, and R. Herschel, "High accuracy position calculation of a hovering uav using a rotating radar," in 2022 19th European Radar Conference (EuRAD). IEEE, 2022, pp. 129–132.
- [16] S. Mohammadi, A. Ghani, and S. H. Sedighy, "Direction-of-arrival estimation in conformal microstrip patch array antenna," *IEEE Transactions on Antennas and Propagation*, vol. 66, no. 1, pp. 511–515, 2017.
- [17] B. R. Jackson, "2d direction of arrival estimation using uniform circular arrays with radiation pattern reconfigurable antennas," *IEEE Access*, vol. 10, pp. 11 909–11 923, 2022.
- [18] B. R. Jackson, S. Rajan, B. J. Liao, and S. Wang, "Direction of arrival estimation using directive antennas in uniform circular arrays," *IEEE Trans. on Antennas and Propag.*, vol. 63, no. 2, pp. 736–747, 2014.
- [19] Y. B. Nechaev and I. Peshkov, "Evaluation of the influence of directivity factor of directive elements of conformal antenna arrays on the performances of azimuth-elevation doa estimation," in 2017 Progress In Electromagnetics Research Symposium-Spring (PIERS). IEEE, 2017, pp. 490–495.
- [20] Q. Shen, W. Liu, W. Cui, and S. Wu, "Underdetermined doa estimation under the compressive sensing framework: A review," *IEEE Access*, vol. 4, pp. 8865–8878, 2016.
- [21] S. Uemura, K. Nishimori, R. Taniguchi, M. Inomata, K. Kitao, T. Imai, S. Suyama, H. Ishikawa, and Y. Oda, "Direction-of-arrival estimation with circular array using compressed sensing in 20 ghz band," *IEEE Antennas and Wireless Propagation Letters*, vol. 20, no. 5, pp. 703– 707, 2021
- [22] K. Schab, E. L. Daly, and J. T. Bernhard, "Direction estimation using compressive array sensing and pattern reconfigurable antennas," in 2013 Asilomar Conference on Signals, Systems and Computers. IEEE, 2013, pp. 927–930.
- [23] G. R. Friedrichs, M. A. Elmansouri, and D. S. Filipovic, "A compact machine learning architecture for wideband amplitude-only direction finding," *IEEE Transactions on Antennas and Propagation*, vol. 70, no. 7, pp. 5189–5198, 2021.
- [24] M. F. Imani and I. Alamzadeh, "Conformal frequency-diverse metasur-face for computational AoA detection," *IEEE Antennas and Wireless Propagation Letters*, vol. 22, no. 11, pp. 2634–2638, 2023.
- [25] T. Williams, "Toward simple dynamic metasurface antennas for reconfigurable beamforming and aoa detection," Master's thesis, Arizona State University, 2024.
- [26] T. Sleasman, M. F. Imani, W. Xu, J. Hunt, T. Driscoll, M. S. Reynolds, and D. R. Smith, "Waveguide-fed tunable metamaterial element for dynamic apertures," *IEEE Antennas and Wireless Propagation Letters*, vol. 15, pp. 606–609, 2015.
- [27] N. Shlezinger, G. C. Alexandropoulos, M. F. Imani, Y. C. Eldar, and D. R. Smith, "Dynamic metasurface antennas for 6g extreme massive mimo communications," *IEEE Wireless Communications*, vol. 28, no. 2, pp. 106–113, 2021.
- [28] T. Sleasman, M. Boyarsky, M. F. Imani, J. N. Gollub, and D. R. Smith, "Design considerations for a dynamic metamaterial aperture for computational imaging at microwave frequencies," *JOSA B*, vol. 33, no. 6, pp. 1098–1111, 2016.
- [29] I. Alamzadeh and M. F. Imani, "Sensing and reconfigurable reflection of electromagnetic waves from a metasurface with sparse sensing elements," *IEEE Access*, vol. 10, pp. 105 954–105 965, 2022.
- [30] —, "Detecting angle of arrival on a hybrid ris using intensity-only data," *IEEE Antennas and Wireless Propagation Letters*, vol. 22, no. 9, pp. 2325–2329, 2023.
- [31] I. Alamzadeh, G. C. Alexandropoulos, and M. F. Imani, "Intensity-only omp-based direction estimation for hybrid reconfigurable intelligent surfaces," in 2023 IEEE International Symposium on Antennas and Propagation and USNC-URSI Radio Science Meeting (USNC-URSI). IEEE, 2023, pp. 01–02.
- [32] M. F. Imani, J. N. Gollub, O. Yurduseven, A. V. Diebold, M. Boyarsky, T. Fromenteze, L. Pulido-Mancera, T. Sleasman, and D. R. Smith, "Review of metasurface antennas for computational microwave imaging," *IEEE transactions on antennas and propagation*, vol. 68, no. 3, pp. 1860–1875, 2020.